EGU General Assembly 2020

Experimental and CDEM Analysis on Crack Propagation Mechanism of Rock-Like Material Containing Flaws Under Uniaxial and Biaxial Compression

May 7, 2020

Yong Li[1,2], Weishen Zhu[2], Chao Wei[2,3], Weibing Cai [1,2], Guannan Wu [1,2], Zhiheng Wang[2,3], Weiqiu Kong [2,3]

(1. School of Qilu Transportation, Shandong Univ., Ji'nan 250061, China; 2. Geotechnical & Structural Eng. Research Center, Shandong Univ., Ji'nan 250061, China; 3. School of Civil Engineering, Shandong Univ.,Ji'nan 250061,China)

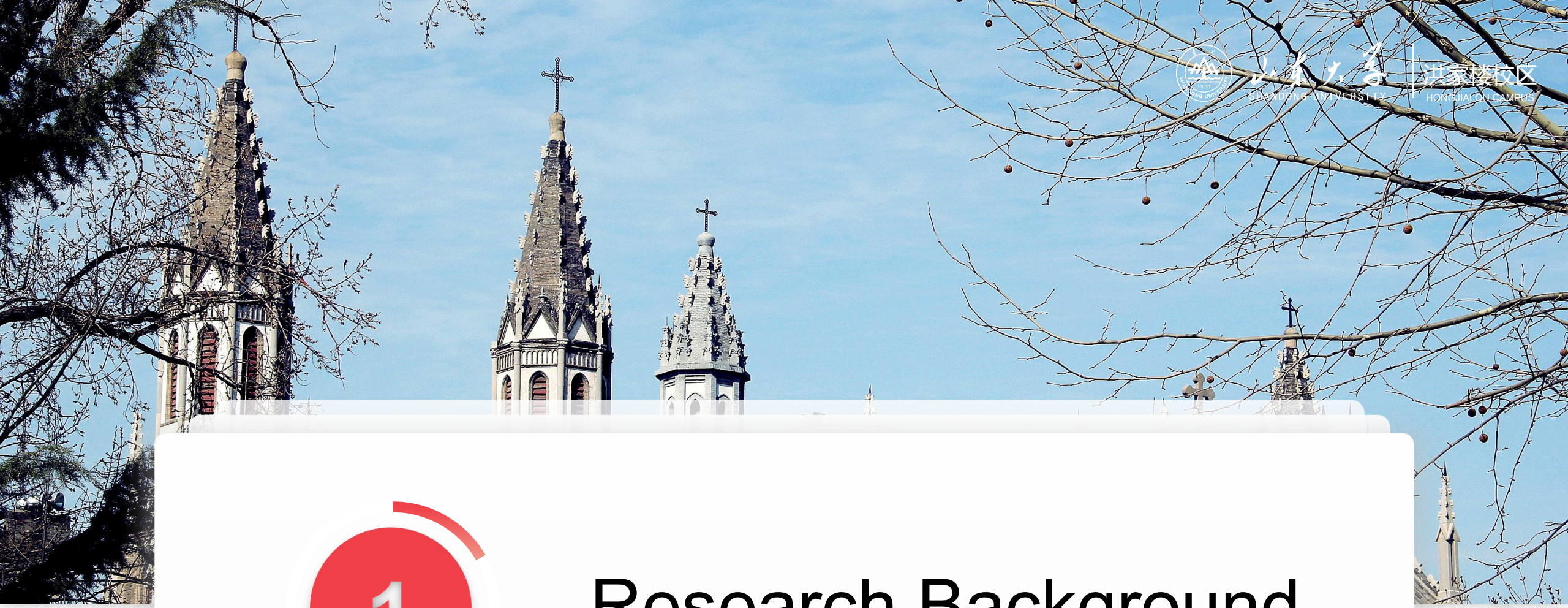

1

Research Background

Research Background

In southwestern China, abundant water resources with potential for electricity generation are being utilized.

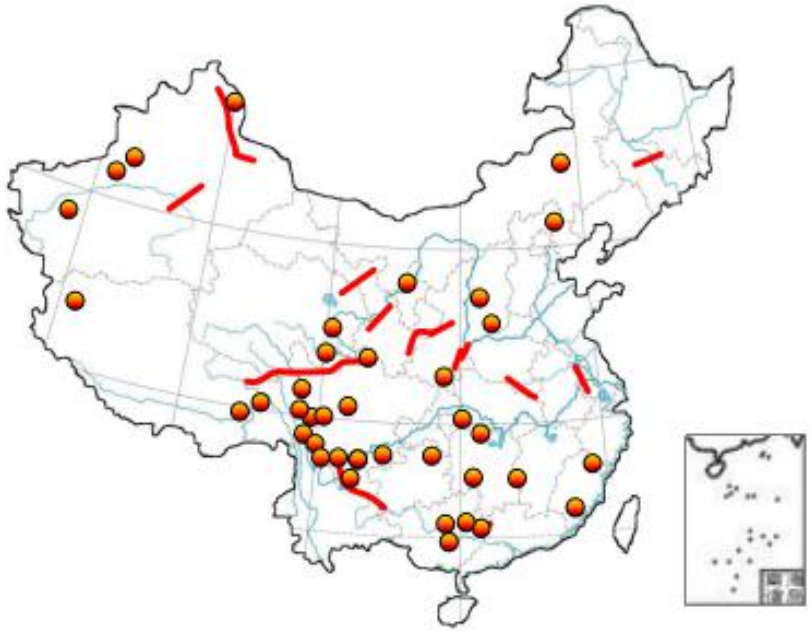

Representative water diversion projects and hydropower projects

Research Background

Underground engineerings are dense and most of them are large-scale, whose geological conditions are mostly complex.

WuDongDe main powerhouse:
L×H×W=333×90×30.5m

Baihetan main powerhouse:
L×H×W=438×88×31m

HuangDeng main powerhouse:
L×H×W=228×76×33m

JinPing main powerhouse:
L×H×W=276×68×25m

Research Background

Underground rock mass conditions are often complex, and rock mass usually contain a large number of joints, fissures, and other geological defects

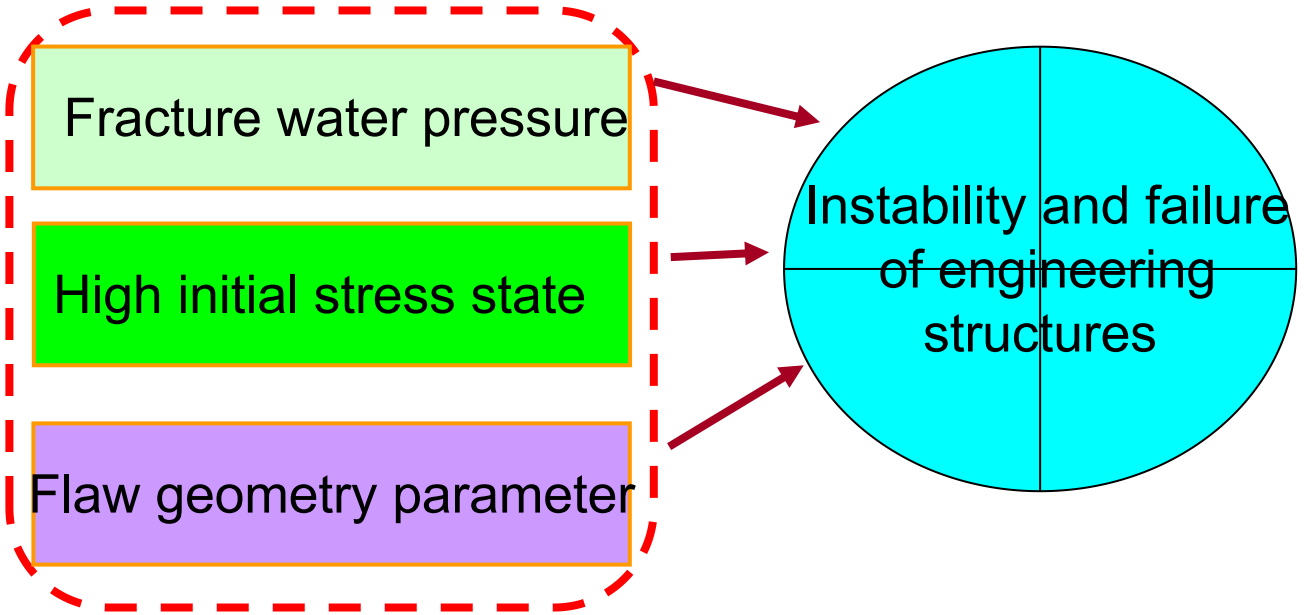

Research Background

Underground engineering, such as tunnels, hydropower stations often pass through sandstone stratum. Sandstone contains a large number of horizontal and inclined flaws.

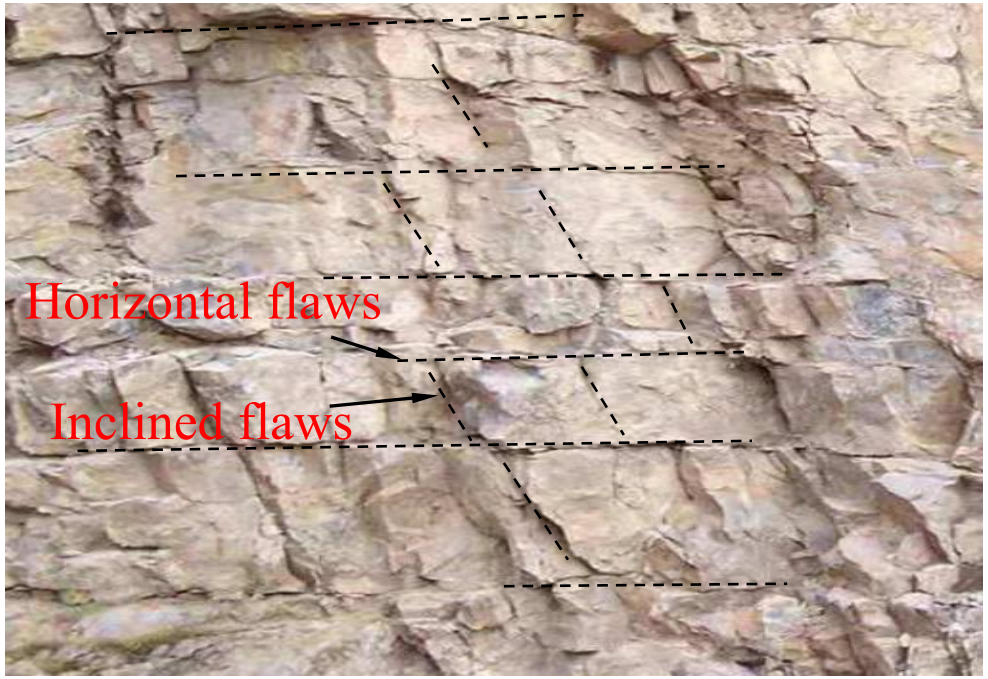

The mechanism of crack propagation and the rock properties need to be further studied under hydraulic coupling.

2 Crack growth tests under complex stress conditions

Experimental results

Geometry of specimen with prefabricated flaws

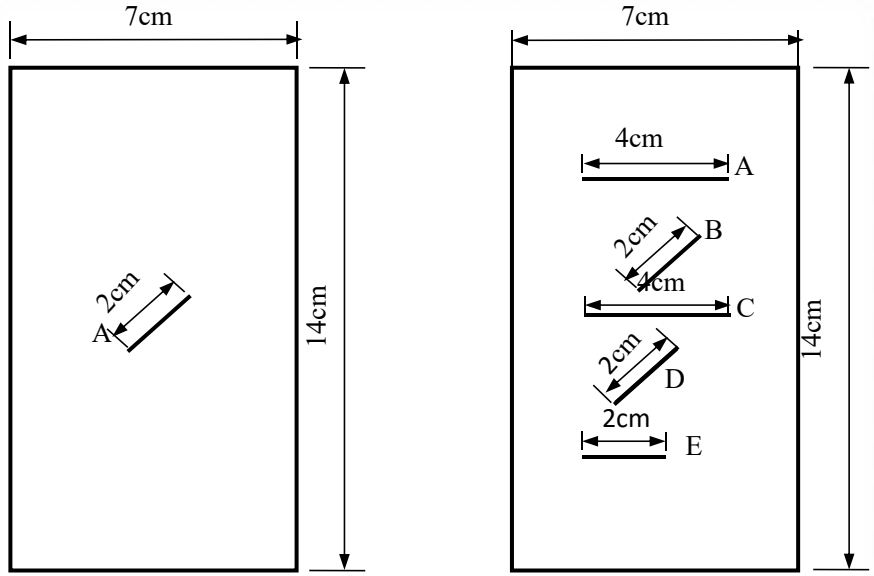

Flaw distribution

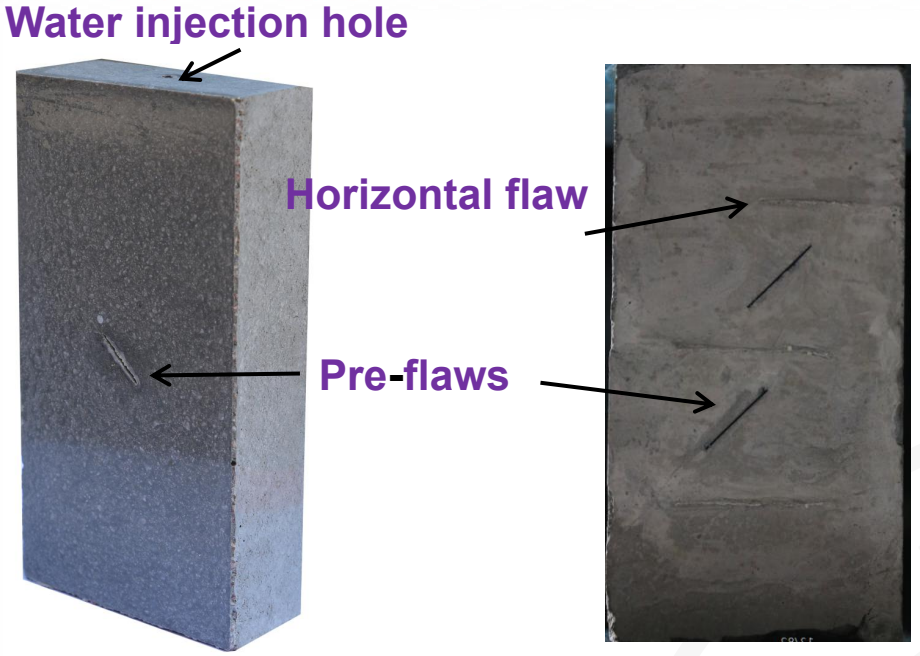

Test specimen

Experimental apparatus:

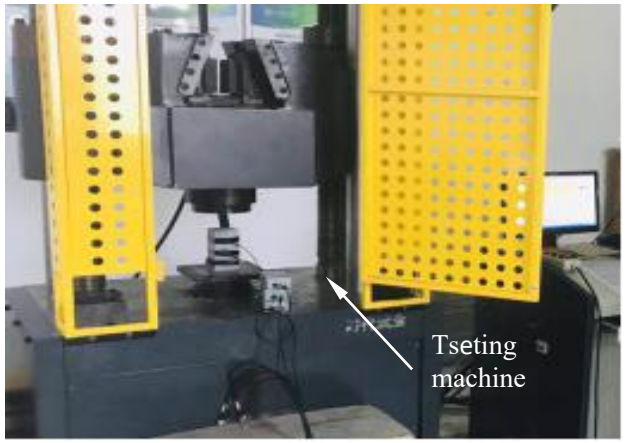

(a)

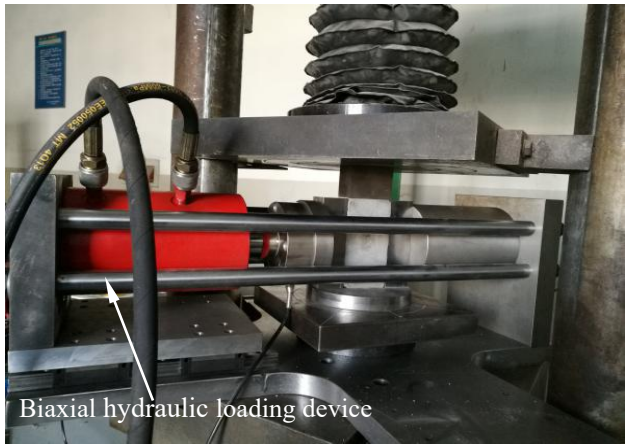

(b)

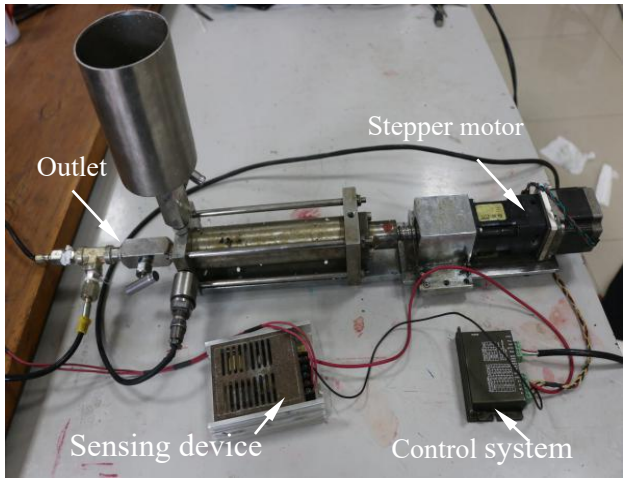

(c)

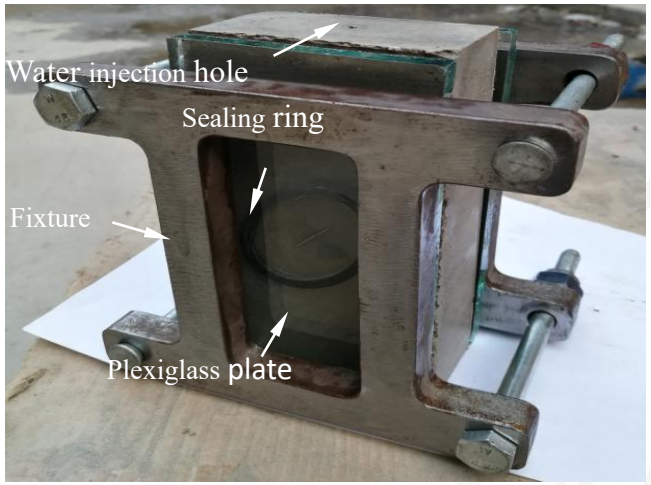

(d)

Experimental apparatus: (a) an electro-hydraulic servo-control testing machine (model number WAW-1000C); (b) a self-made biaxial hydraulic loading device; (c) a fissure water injection apparatus; (d) a set of fixtures to sealing the pressured water on the surface of a specimen.

Experimental results

Two parallel inclined flaws and horizontal flaws under uniaxial compression

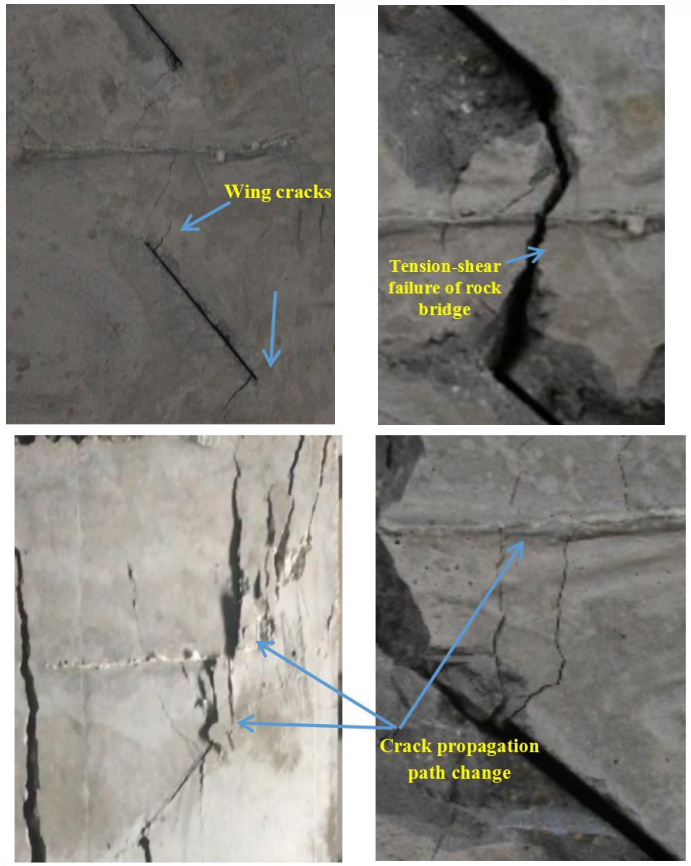

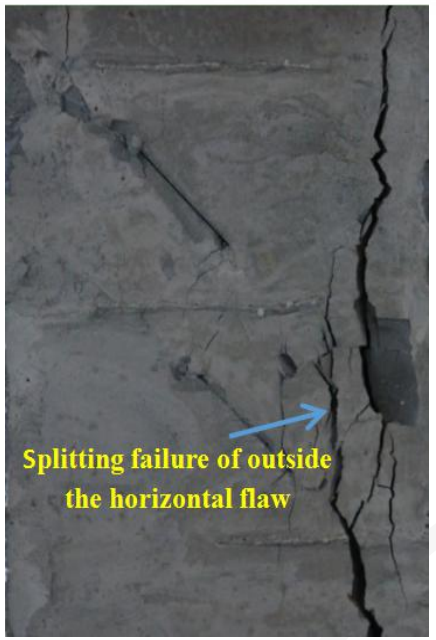

The rock bridge has undergone a tension-shear failure

When the wing cracks and secondary shear cracks at the end of the inclined flaws extend through the horizontal flaw, the extension path of the wing crack and the secondary crack has been changed.

Experimental results

Two parallel inclined flaws and horizontal flaws under biaxial compression(3MPa)

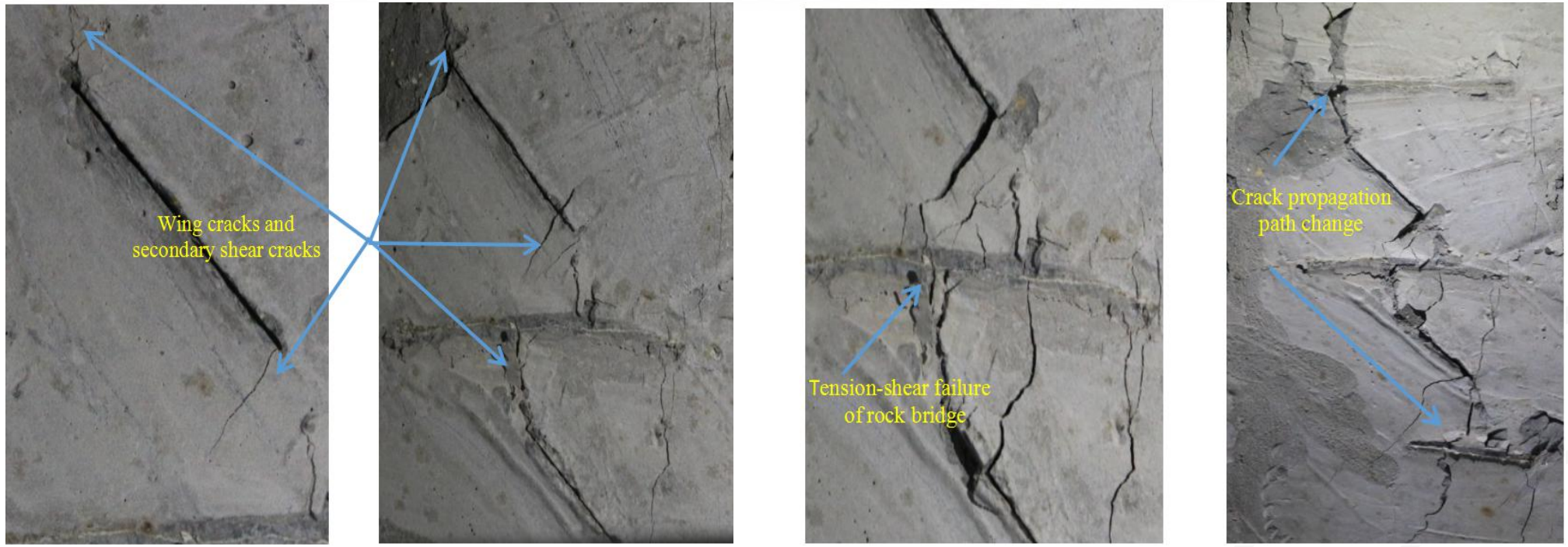

The wing cracks do not penetrate the horizontal flaw, the secondary shear cracks penetrate the horizontal flaw, and the crack propagation path has been changed.

Experimental results

Two parallel inclined flaws and horizontal flaws under biaxial compression(6MPa)

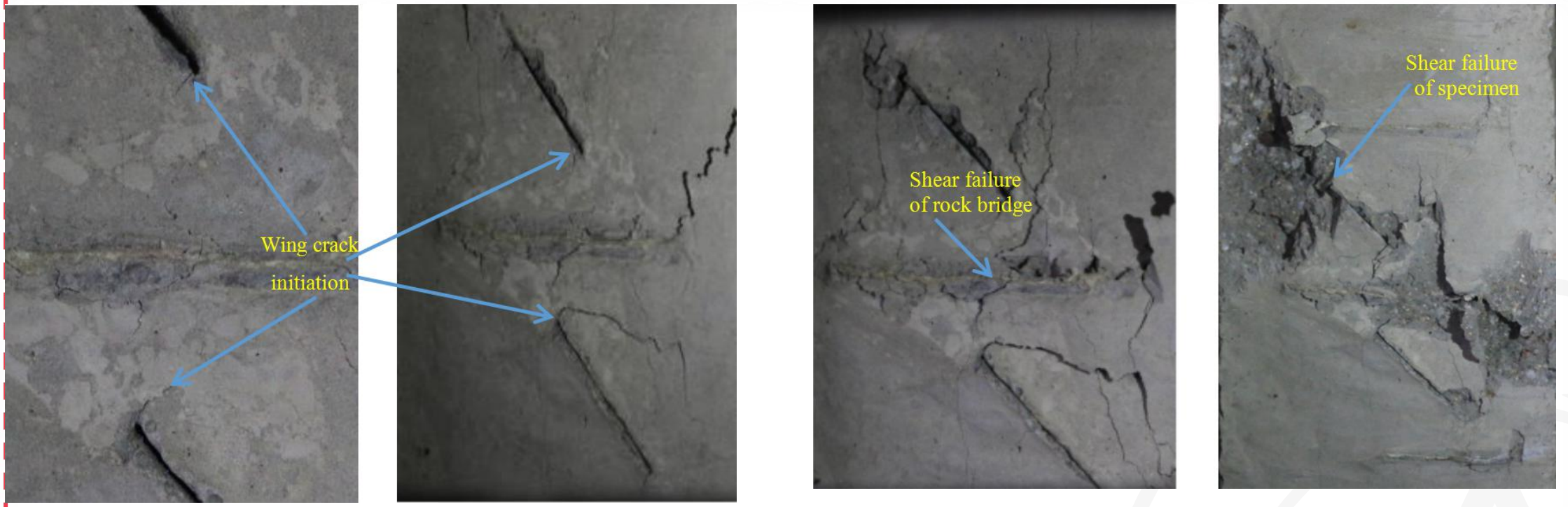

Shear failure occurs at the rock bridge and the wing cracks at the rock bridge are not totally penetrated. At the high lateral pressure, the propagation of wing cracks is restrained, and the crack initiation length is limited. The specimen undergoes shear failure.

Experimental results

Specimens with an inclined flaw under uniaxial compression and different internal water pressures.

(a)Water pressure 1MPa

(b)Water pressure 1MPa

(c)Water pressure 1MPa

The initiation stress and the initiation angle of the wing crack are gradually reduced.

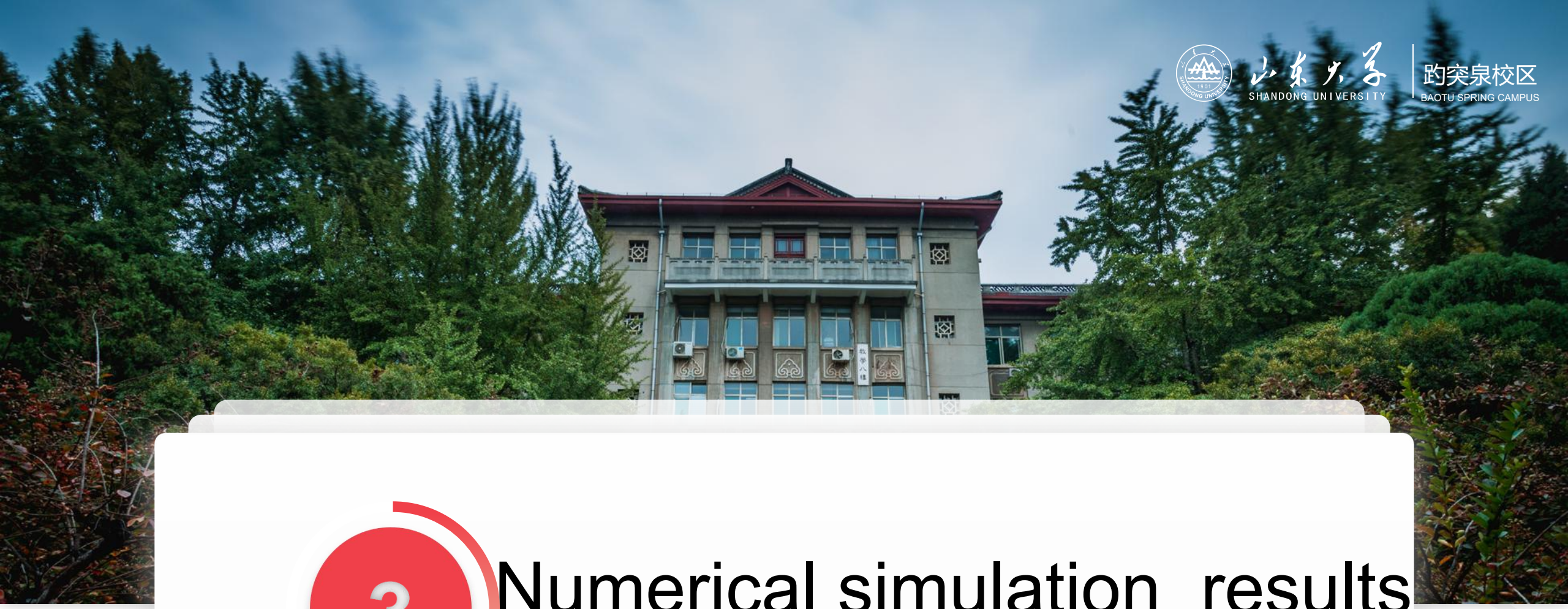

3 Numerical simulation results

Numerical simulation results

The algorithms of CDEM

- Finite element
- Discrete element method

→ Analysis of progressive failure of rock mass

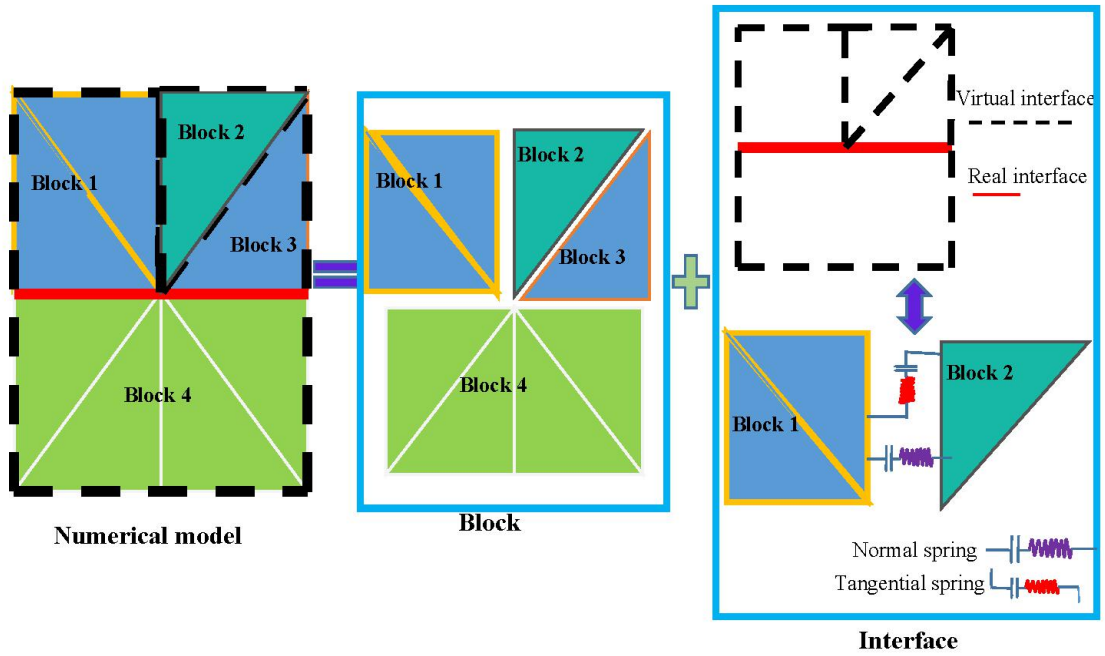

A numerical model in CDEM

The numerical model in CDEM consists of two parts: the block and the interface. A block consisting of one or more finite elements.The common boundary between two blocks is the interface

Numerical simulation results

The algorithms of CDEM

Governing equation: $M\ddot{u} + C\dot{u} + Ku + K_c u_c + C_c \dot{u}_c = F$

For the node forces contributed by the interface, when the block maintains a continuous medium：

$$F_n = -K_n \Delta u_n$$

$$F_s = -K_s \Delta u_s$$

Maximum tensile stress criterion:

$$\sigma_n \geq \bar{\sigma}_n$$

Mohr Coulomb strength criterion:

$$\tau \geq \sigma_n \tan \varphi + c$$

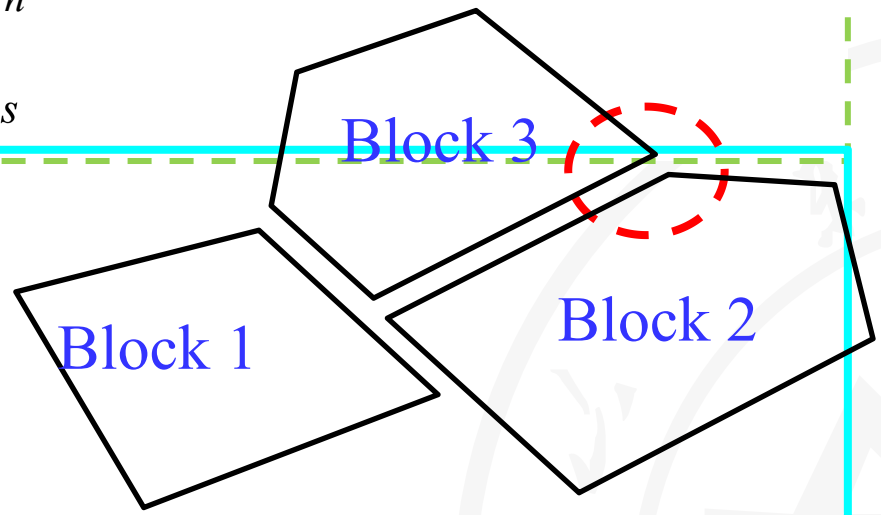

Numerical simulation results

Seepage equation of fracture network

$$\begin{cases} \vec{v} = -\boldsymbol{K} \cdot \nabla h \\ \nabla \cdot \vec{v} = S \dfrac{\partial h}{\partial t} \end{cases}$$

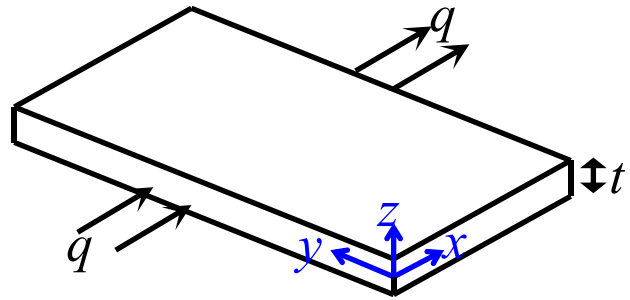

$$\begin{cases} K_x \dfrac{\partial^2 h}{\partial x^2} + K_y \dfrac{\partial^2 h}{\partial y^2} = S \dfrac{\partial h}{\partial t} & in \quad \Omega_f \\ h = \overline{h} & on \quad \Gamma_{fh} \\ K_x \dfrac{\partial h}{\partial x} n_x + K_y \dfrac{\partial h}{\partial y} n_y = \overline{q} & on \quad \Gamma_{fq} \end{cases}$$

Permeability coefficient

$$K_x = K_y = \frac{\rho g t^3}{12\,\mu}$$

Numerical simulation results

Two parallel inclined flaws and horizontal flaws under uniaxial and biaxial compression

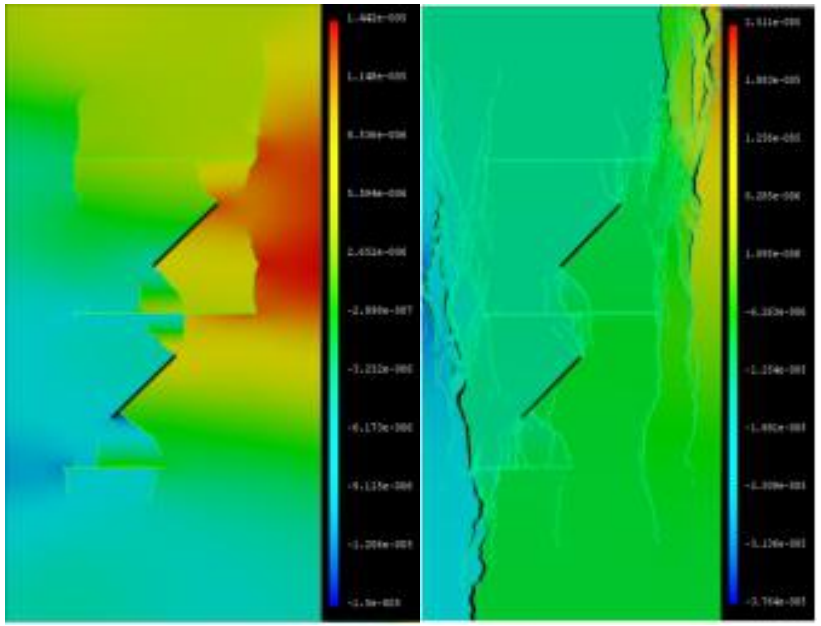

Crack propagation under uniaxial compression

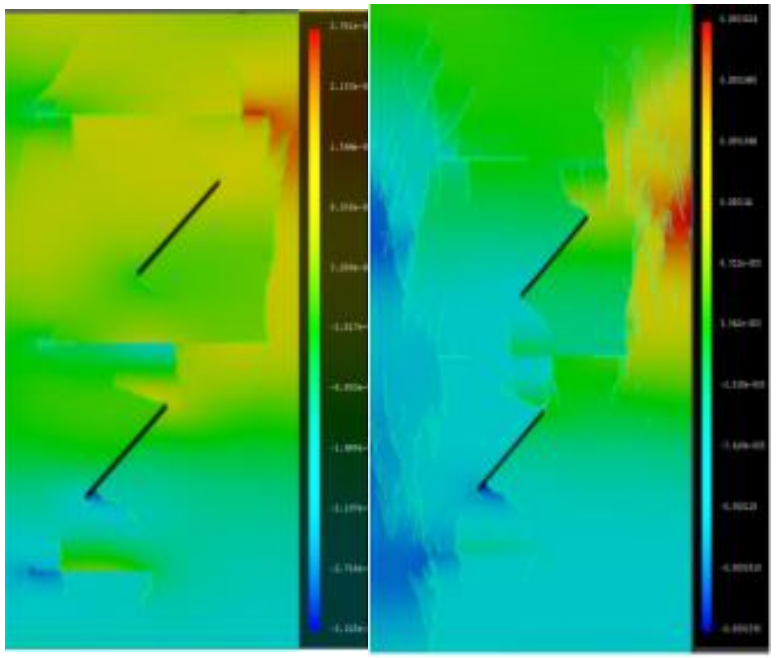

with a lateral pressure of 3 MPa

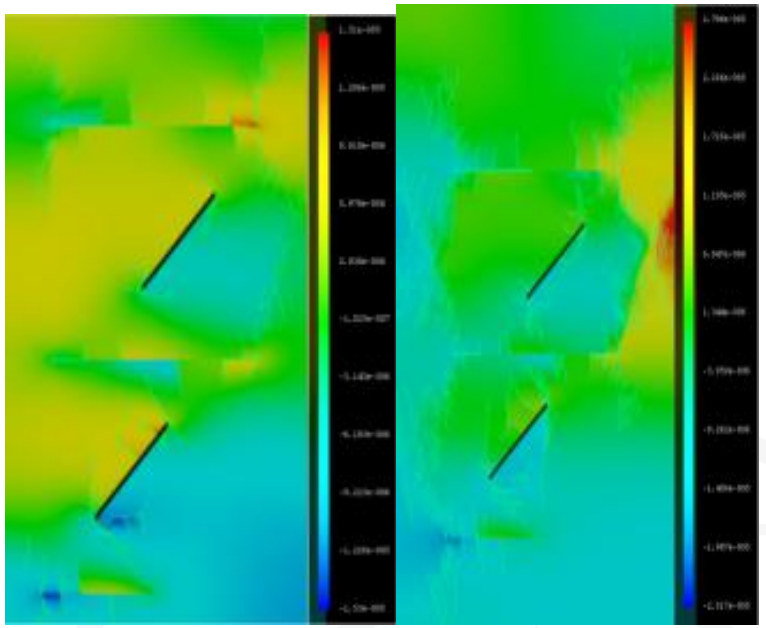

with a lateral pressure of 6 MPa

Crack propagation on specimens containing two parallel inclined flaws and horizontal flaws under uniaxial and different lateral pressures simulated by CDEM.

Numerical simulation results

Two parallel inclined flaws and horizontal flaws under uniaxial and biaxial compression

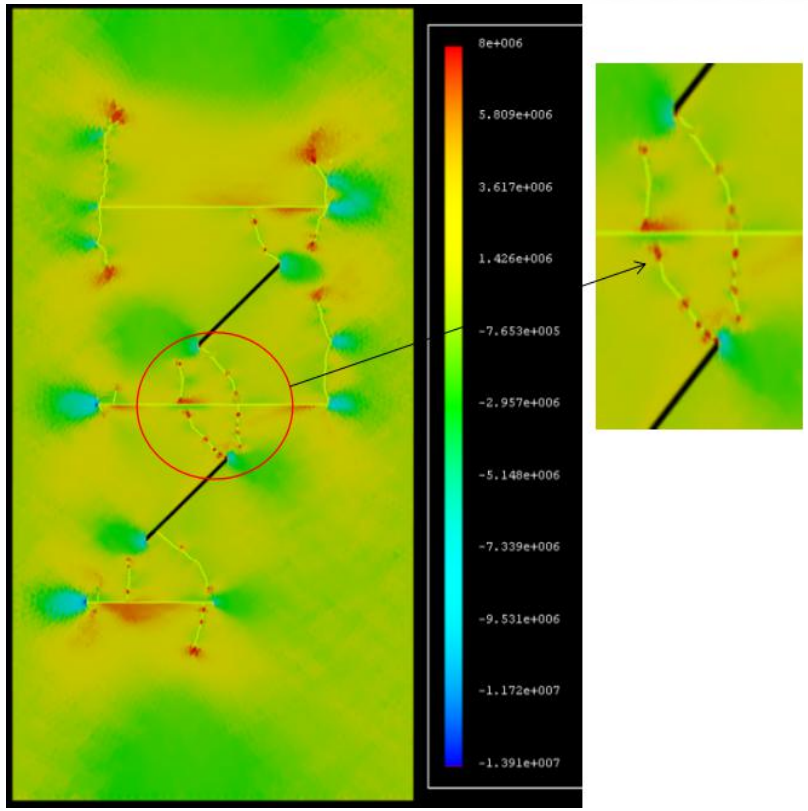

Uniaxial compression

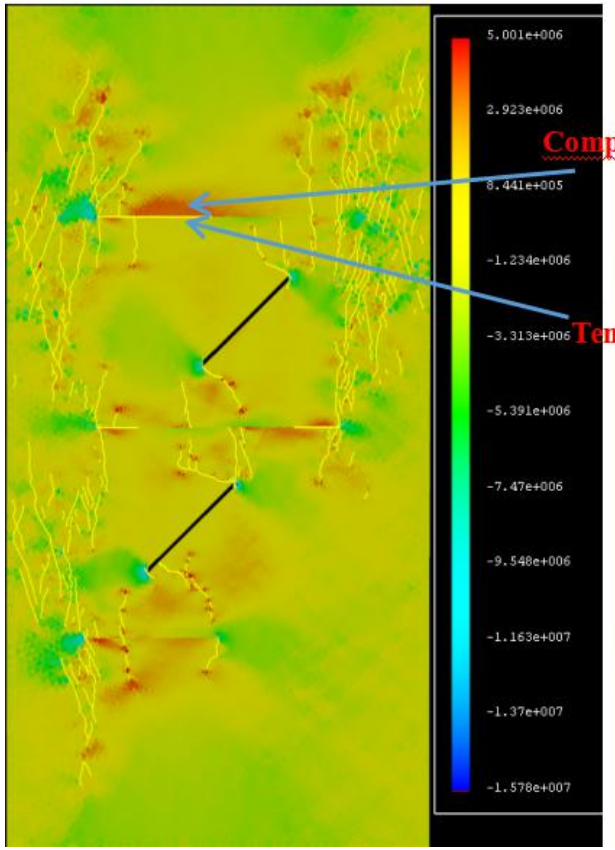

Lateral pressure 3 MPa

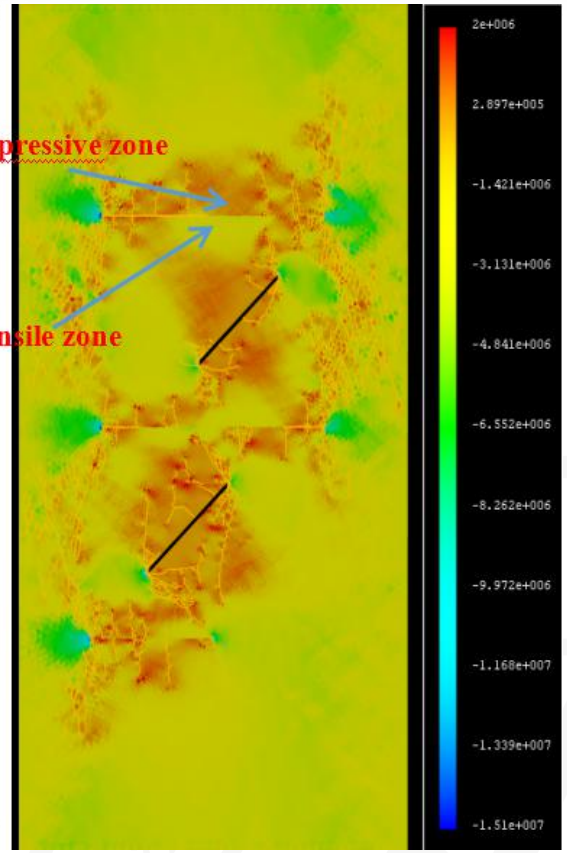

Lateral pressure 6 MPa

A tensile-stress zone appears at the top of the horizontal flaw. When the tensile stress in this zone reaches the tensile strength of the geo-material, the tensile crack (mode I crack) will appear in this zone

Numerical simulation results

An inclined flaw under uniaxial compression and different internal water pressures

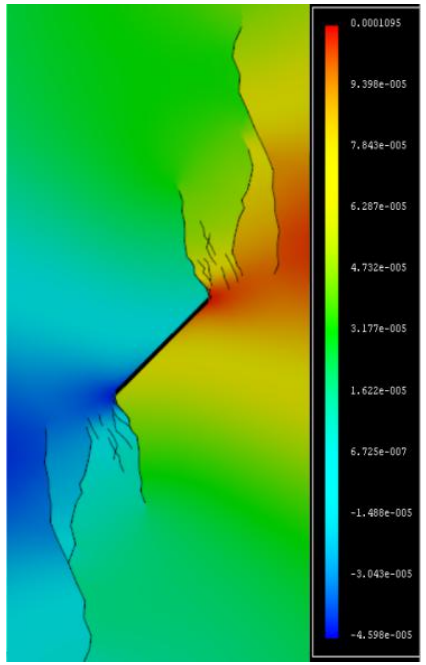

Water pressure 0.5 MPa

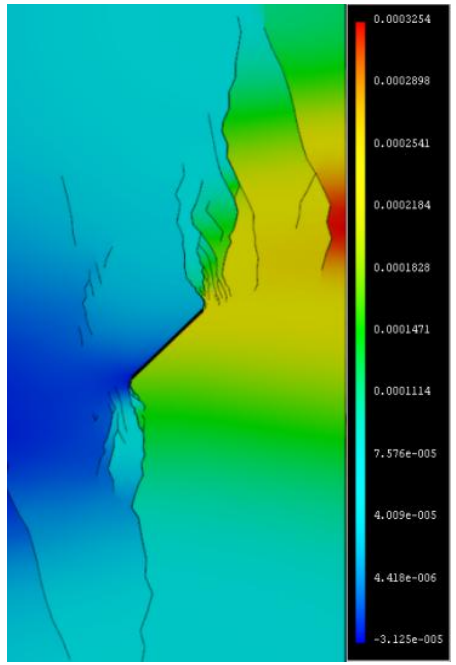

Water pressure 1 MPa

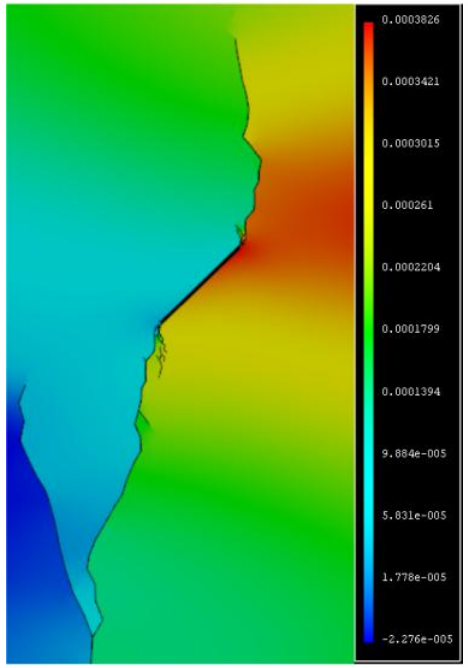

Water pressure 2 MPa

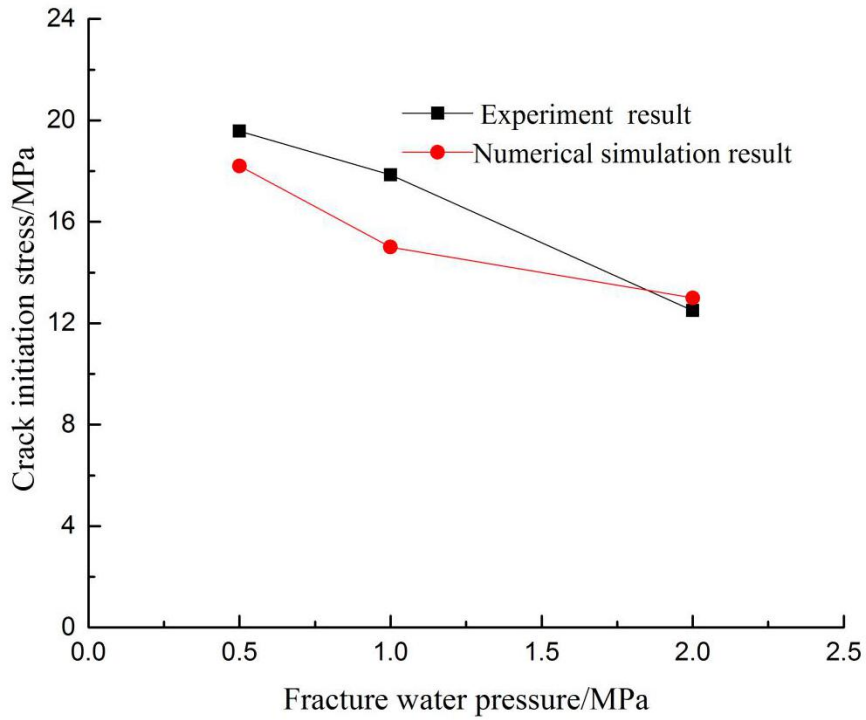

Crack propagation and coalescence on specimens with an inclined flaw under uniaxial compression and different internal water pressures

Numerical simulation results

An inclined flaw under uniaxial compression and different internal water pressures

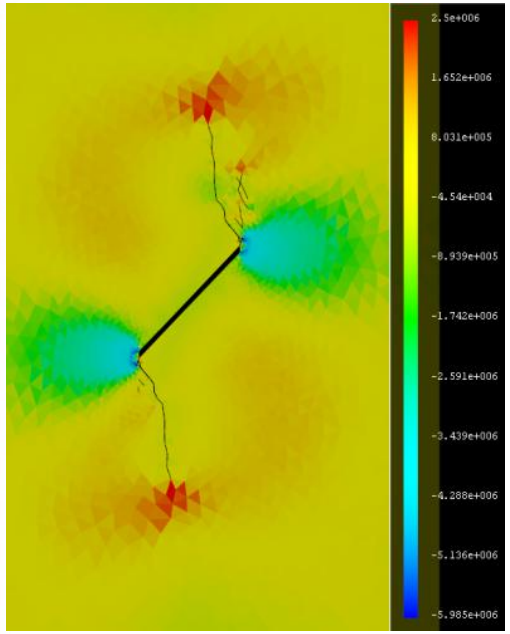

Water pressure 0.5 MPa

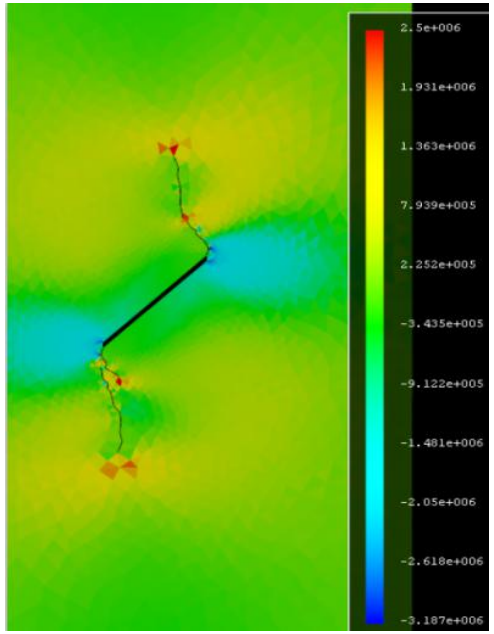

Water pressure 1 MPa

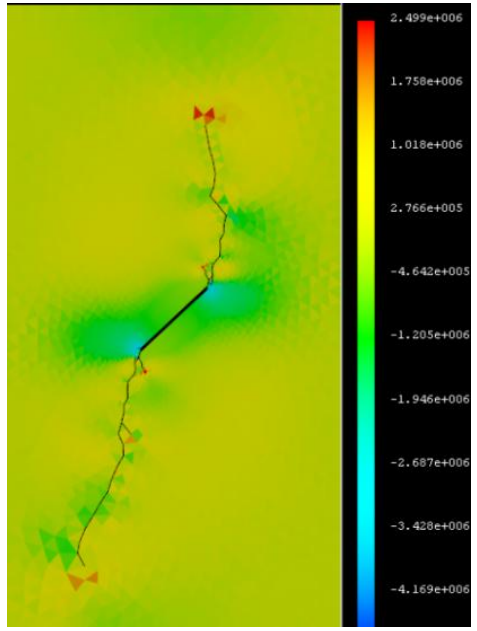

Water pressure 2 MPa

With the increase of the water pressure, the range of the two sides of the flaw compressed by the internal water pressure becomes larger and larger. The disturbed stress field owing to internal water pressure results in the change of the initial stress field at the crack tip.

Change process of maximum principal stress field at the tip of wing cracks under different internal water pressures

Numerical simulation results

Inclined flaws with internal water pressure and horizontal flaws without internal water pressure

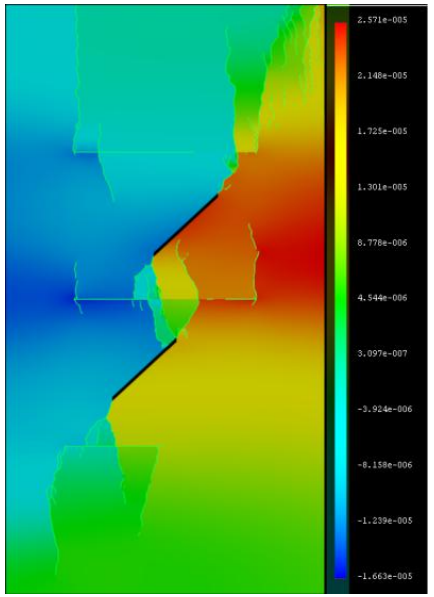

Water pressure 0.5 MPa

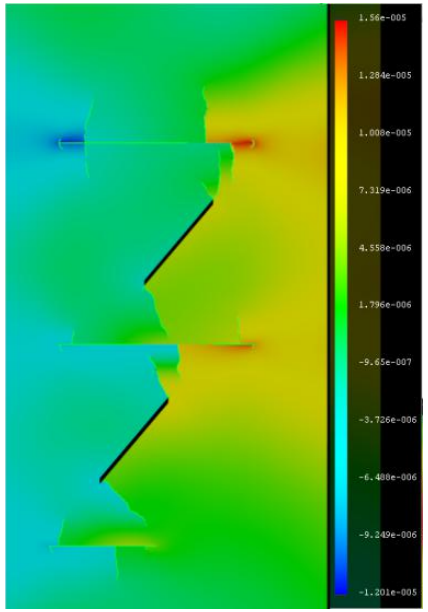

Water pressure 1 MPa

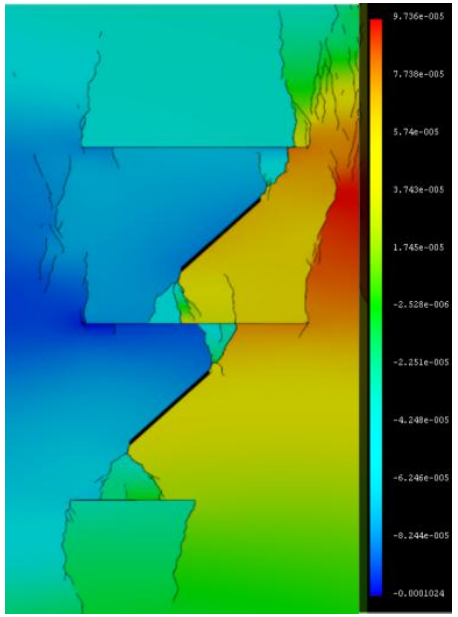

Water pressure 2 MPa

Uniaxial compressions

The crack initiation is much faster than that under no internal water pressure, and the inflow of internal pressured water after the crack growth increases the crack growth rate

Specimens containing two parallel inclined flaws with internal water pressure and horizontal flaws without internal water pressure under uniaxial compressions.

Numerical simulation results

Inclined flaws with internal water pressure and horizontal flaws without internal water pressure

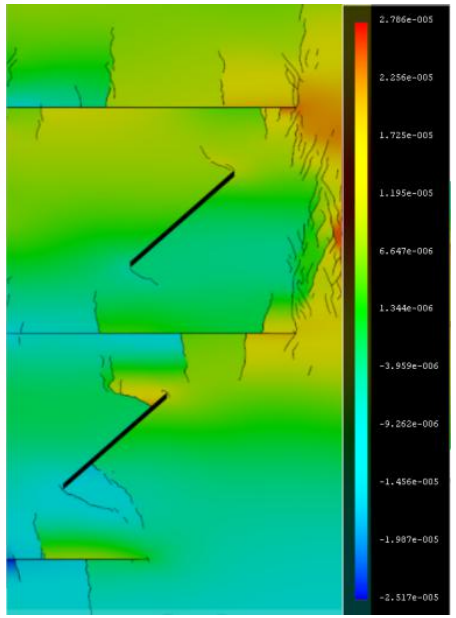

Water pressure 0.5 MPa

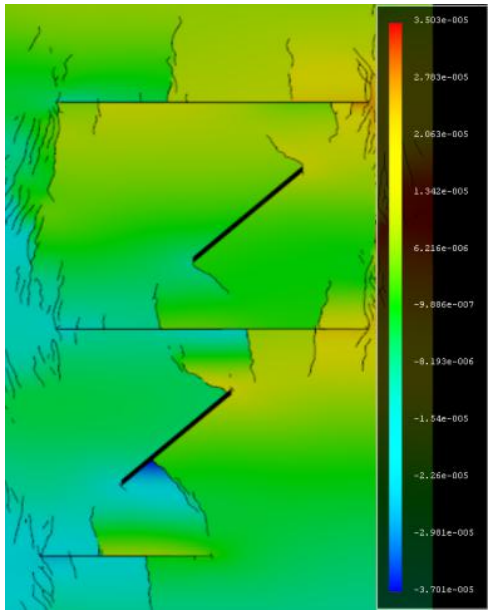

Water pressure 1 MPa

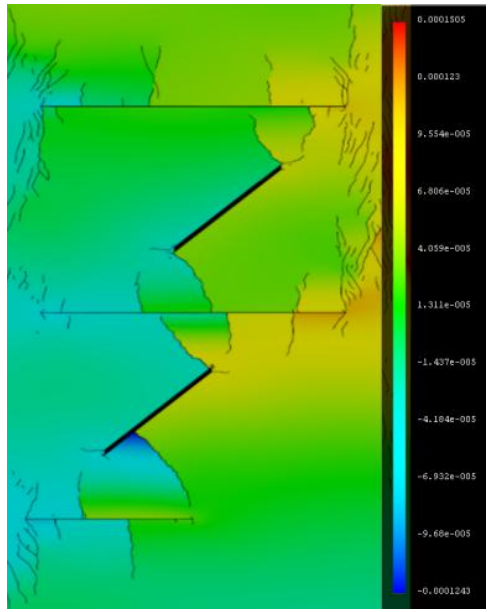

Water pressure 2 MPa

Lateral pressure 3 MPa

When the internal water pressure is low, the existence of lateral pressure restrains the growth of wing cracks. When the specimen is damaged, the wing cracks do not penetrate the horizontal flaws. With the increase of the internal water pressure, the inhibition of the lateral pressure is weakened. Shear cracks are initiated at the end of the flaws

Specimens containing two parallel inclined flaws with internal water pressure and horizontal flaws without internal water pressure under biaxial compressions.

Conclusions

(1) It can be concluded from laboratory tests: under the condition of uniaxial compression, the propagation path and direction of preexisting flaws change obviously after the inclined flaws meet the horizontal flaws during the propagation process, and the phenomenon of ‘displacement jumping’ appears.

(2) It can be concluded from laboratory tests: under the condition of biaxial compression, the increase of lateral pressure suppresses the crack initiation and the development of secondary cracks at the ends of the inclined flaws. The crack initiation stress of wing cracks and the peak strength of the specimen have been greatly increased, and the failure mode of the specimen changes from splitting failure to shear failure.

Conclusions

(3) It can be concluded from laboratory tests: under the combined action of internal water pressure and far-field stress, with the increase of internal water pressure, the maximum principal stress distribution at the tip of wing crack in uniaxial compression gradually decreases, and the initiation stress, initiation angle and peak strength are also gradually reduced.

(4) The CDEM codes have been applied to numerically simulate all the conditions carried out in the laboratory tests and relevant numerical results have been compared with laboratory test results. Although both of the results cannot be totally consistent, numerical simulation results can be basically in agreement with the laboratory test results. Therefore, it can be concluded that the CDEM codes can describe the progressive failure process of geo-materials containing flaws subjected to hydraulic pressure and far-field stress.

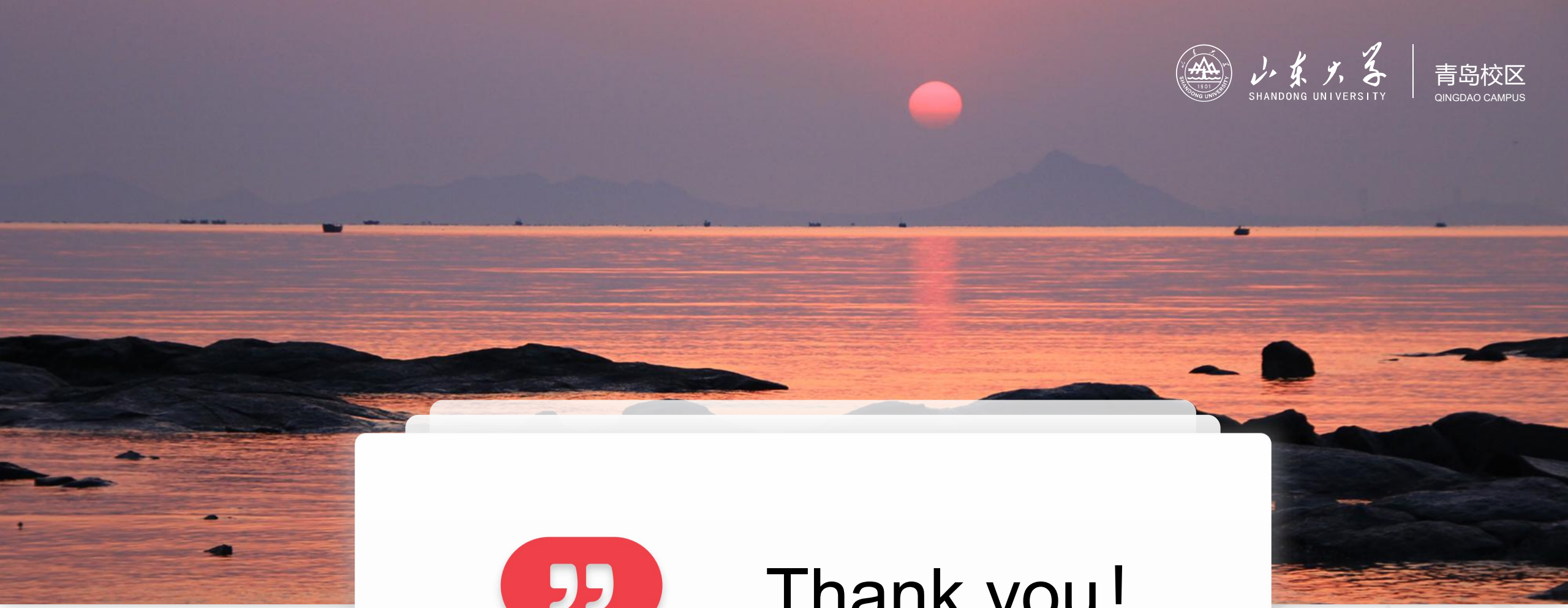

Thank you!